



## Convective tissue movements play a major role in avian endocardial morphogenesis

Anastasiia Aleksandrova<sup>a</sup>, Andras Czirók<sup>a,b</sup>, Andras Szabó<sup>a,b,1</sup>, Michael B. Filla<sup>a</sup>, M. Julius Hossain<sup>c</sup>, Paul F. Whelan<sup>c</sup>, Rusty Lansford<sup>d</sup>, Brenda J. Rongish<sup>a,\*</sup>

<sup>a</sup> Department of Anatomy and Cell Biology, University of Kansas Medical Center, Kansas City, KS 66160, USA

<sup>b</sup> Department of Biological Physics, Eotvos University, Budapest, Hungary

<sup>c</sup> Center for Image Processing and Analysis, Dublin City University, Dublin, Ireland

<sup>d</sup> Biological Imaging Center, California Institute of Technology, Pasadena, CA 91125, USA

### ARTICLE INFO

#### Article history:

Received for publication 1 July 2011

Revised 13 December 2011

Accepted 14 December 2011

Available online 4 January 2012

#### Keywords:

Endocardium

Embryo

Morphogenesis

Quail

Time-lapse

Cardiovascular

Imaging

### ABSTRACT

Endocardial cells play a critical role in cardiac development and function, forming the innermost layer of the early (tubular) heart, separated from the myocardium by extracellular matrix (ECM). However, knowledge is limited regarding the interactions of cardiac progenitors and surrounding ECM during dramatic tissue rearrangements and concomitant cellular repositioning events that underlie endocardial morphogenesis. By analyzing the movements of immunolabeled ECM components (fibronectin, fibrillin-2) and TIE1 positive endocardial progenitors in time-lapse recordings of quail embryonic development, we demonstrate that the transformation of the primary heart field within the anterior lateral plate mesoderm (LPM) into a tubular heart involves the precise co-movement of primordial endocardial cells with the surrounding ECM. Thus, the ECM of the tubular heart contains filaments that were associated with the anterior LPM at earlier developmental stages. Moreover, endocardial cells exhibit surprisingly little directed active motility, that is, sustained directed movements relative to the surrounding ECM microenvironment. These findings point to the importance of large-scale tissue movements that convect cells to the appropriate positions during cardiac organogenesis.

© 2012 Elsevier Inc. All rights reserved.

### Introduction

Vertebrate heart morphogenesis, the assembly of a midline tubular heart from bilateral precursor fields, results from an elaborate interplay of events that occur at molecular, cellular and tissue levels of organization. The resulting heart tube is comprised of an inner layer of endocardium separated from the outer myocardium by a layer of extracellular matrix (ECM) termed the cardiac jelly. The interactions between cardiac progenitors and the surrounding ECM during morphogenetic movements are a critical aspect of the development process: the cardiac ECM is involved in the proliferation, differentiation, survival, communication and migration of cardiac cells—by providing an adhesion substrate and sequestering growth factors (Bowers and Baudino, 2010).

Tubular heart assembly takes place in the swiftly-moving environment of the forming foregut. The cardiac splanchnic mesoderm is physically coupled to the underlying endoderm that will form the ventral floor of the foregut. Both structures remain transiently

connected via a mesentery until heart looping commences. In addition to tissue movements underlying the elongation of the foregut, the formation of the heart tube also involves substantial rearrangements of myocardial and endocardial precursors (reviewed in Linask, 2003).

Little is known regarding the origin and movements of the endocardial precursors as they form the inner layer of the heart, continuous with the endothelial lining of blood vessels. It is widely believed that endocardial cells share a common precursor with the myocardial cells, but diverge to form a distinct lineage with some shared characteristics of endothelial cells (Harris and Black, 2010; Linask, 2003). The exact time and place of this divergence is unknown, but studies in avian embryos indicate that the two cell lineages segregate prior to or at early gastrulation; i.e. before these cells populate the primary heart field at HH stage 4 (reviewed in Ishii et al., 2009). The endocardial precursors differentiate and move into an ECM-rich microenvironment located between the splanchnic mesoderm and endoderm. However, the relationship of mesodermal and endodermal tissue level movements to movements of the endocardial precursor population is largely unknown.

In this study, we establish the morphogenetic movements of both the endocardial precursor cells and ECM fibrils in their microenvironment. We show that the endocardial tube in an amniote (avian) embryo forms and elongates as a consequence of large-scale tissue movements, which carry both endocardial progenitors and their

\* Corresponding author at: Anatomy and Cell Biology, Lied 3043, University of Kansas Medical Center, 3901 Rainbow Blvd., Kansas City, KS 66160, USA. Fax: +1 913 588 2710.

E-mail address: [brongish@kumc.edu](mailto:brongish@kumc.edu) (B.J. Rongish).

<sup>1</sup> Current address: Centrum Wiskunde en Informatica, Amsterdam, The Netherlands and Netherlands Consortium for Systems Biology, The Netherlands.

local ECM environment into the forming heart. As a consequence, ECM filaments, originally associated with the anterior LPM are transferred medially where the fibrils incorporate into the cardiac jelly. We also find that the transport of endocardial progenitors is mostly a passive process; their autonomous migration relative to the ECM microenvironment is limited and can be characterized as a slightly-biased random walk.

## Materials and methods

### Quail embryo preparation

Fertile wild type (*Coturnix coturnix japonica*) or Tie1::H2B-YFP (Sato et al., 2010) quail eggs (Ozark Egg Co., Stover, MO) were incubated for varying periods of time (from 20 to 36 h) at 37 °C to reach stages HH6 to HH11 (Hamburger and Hamilton, 1951). Embryos were then isolated and cultured as in Cui et al. (2009) (modified EC culture; Chapman et al., 2001).

### Immunofluorescent labeling of ECM and endothelial/endocardial cells, *in vivo*

Monoclonal antibodies directed against fibrillin-2 and fibronectin ECM proteins (JB3, B3D6; DSHB, Iowa City, IA) or a quail endothelial cell surface marker (QH1; Pardanaud et al., 1987; DSHB) were directly conjugated to AlexaFluor 488, 555 or 647 (Molecular Probes) according to the manufacturer's instructions. The direct conjugates were injected into the lateral plate mesoderm as 5–40 nl boluses using a PLI-100 (Harvard Instruments) microinjector as described in Little and Drake (2000). Microinjections were performed 30–60 min prior to the beginning of the image acquisition to allow for antibody diffusion and antigen binding.

### Wide-field time-lapse imaging

Automated microscopy of immunolabeled quail embryos was performed as described elsewhere (Czirók et al., 2002; Zamir et al., 2008). To enhance contrast, selected epifluorescence image stacks were deconvolved by a commercial, blind adaptive deconvolution software (Autoquant X, MediaCybernetics). Manual tracing of image details, notably the ECM filaments, was performed using custom software (see, e.g., Czirók et al., 2004). As Fig. 3 of Czirók et al., (2004) and Supplemental Fig. 1 demonstrates, despite overall changes in ECM organization, the details used to track ECM filaments (such as filament branch points or shapes) are clearly recognizable from frame to frame. The spatial extent of the recognizable features (up to 10 µm) is much smaller than the traced displacements (200 µm to 1 mm). The size of the tracked features thus limits the spatial resolution of the trajectories, but only to an extent comparable to the line width used in the images to represent them.

### Post-fixation immunofluorescence labeling

Embryos were fixed and prepared for immunolabeling according to Little and Drake (2000). Monoclonal antibodies against avian epitopes (JB3, B3D6, QH1), directly conjugated to AlexaFluor 488, 555 or 647, were added at 1:1000 dilutions in 3% BSA for overnight incubation. Nuclei were counterstained with 4',6-diamidino-2-phenylindole (DAPI) at 300 nM in PBS. Frozen sections were incubated in 0.5 M (NH<sub>4</sub>)<sub>2</sub>SO<sub>4</sub> for 30 min to remove paraformaldehyde-induced autofluorescence and rinsed with PBS. Subsequently non-specific epitopes were blocked by incubation in 3% BSA solution in PBS for 1 h. Monoclonal antibodies against ECM epitopes were added at 1:1000 dilutions in 3% BSA for 2 h of incubation. For confocal and epifluorescent imaging whole embryo specimens and sections were mounted on slides with ProLong Gold antifade reagent (Molecular Probes).

### Confocal imaging

Confocal imaging of whole-mount embryo specimens was performed using a Nikon 90i upright microscope with a Nikon C1 confocal scan head and Nikon Plan Apochromat 10× and 20× objectives.

### Preparation of transverse cryosections

Embryos were fixed in 3% paraformaldehyde for 30 min. Then tissue was rinsed in PBS and subjected to a sucrose gradient (5%, 15%, 30% in PBS), embedded in OCT (Sakura Finetek USA, Inc, Torrance, CA) and stored at –80 °C. Subsequently 10 µm transverse sections were prepared from frozen blocks using a Leica CM3050 cryostat.

### Particle Image Velocimetry (PIV) analysis

We used the two step algorithm of Zamir et al., 2005; implemented in MatLab (Mathworks, Inc.) and further detailed in Supplemental Figs. 2D, E. Briefly, images were divided into overlapping tiles, each 75 µm wide. The displacements of the tiles were determined by cross-correlation analysis; for each tile we searched the next image for the location that exhibited the most similar intensity pattern. The resulting displacement vectors were then interpolated and denoised by a thin-plate spline fit, yielding our coarse displacement map. This map was used to construct a second, higher resolution one. The cross-correlation procedure was repeated with tiles that were only 30 µm wide. To reduce ambiguities associated with smaller tiles (patterns within smaller tiles are less unique), the subsequent image was scanned only in the vicinity of positions predicted by the coarse map. In this study we did not apply a final smoothing (spline fitting) step, but kept the results of the second cross-correlation analysis.

Within the whole embryo, the ECM label was highly non-uniform, as some areas were exposed to more antibody than others. Image tiles corresponding to areas where the immunofluorescence was weak are very noisy; hence the cross correlation analysis was more error-prone. To reflect this, for each PIV-derived displacement vector we assigned a weight, the local standard deviation of fluorescence intensity. Thus, displacement vectors characterizing a detail-rich region carry more weight in the subsequent analyses than those obtained in a weakly-labeled area (see Supplemental Fig. 2E).

### Automated cell tracking

To track fluorescent nuclei in 3D within a series of image stacks, a novel algorithm, referred to as the CIPA tracker, was developed (Hossain et al., 2011). Briefly, the algorithm automatically detects a set of prominent cells in the image stack as bright objects, using a multi-stage segmentation approach (see Supplemental Fig. 2H). To identify the same cell within a consecutive pair of images, objects that are located within a certain distance are compared by several measures, such as size, brightness or texture similarity. In addition to in-plane searches, the program also probes the two immediately adjacent optical planes to deal with object motion along the z-axis.

### Motion analysis

To characterize ECM and cell rearrangements at various stages of heart development, pairs of deconvolved image stacks were selected. The images within the stacks were taken 20 min apart. A given pair, *P*, was analyzed through the following procedure. By manual masking (see Supplemental Fig. 2C), two additional image stack pairs were derived: one containing the forming heart, the other the somites or the pre-somitic mesoderm (to be used as a reference). The corresponding optical sections and fluorescence channels were compared by PIV analysis as described above. For automated (CIPA) tracking

we used all available recorded image stacks within the *time interval separating the image pair*,  $P$ . Velocities (displacements normalized by the time lag between the images of  $P$ ) were presented in a reference system co-moving with the somites. Thus, we use the term “velocity” to describe a vector-value characterizing both the rate and direction of the displacements of selected objects. The term “speed” is used to describe the magnitude of the velocity vector.

Active cell velocities were calculated as the local vectorial difference between the cell- and ECM-derived velocity vectors (Supplemental Figs. 2G, I). The “reliability” weight assigned to the vectorial difference is the lesser of the two weights assigned to the vectors. As the CIPA-predicted displacement vectors may point in various directions, even within a small area, we obtained the locally prevalent direction and speed of active motion by replacing each vector by a local average within a radius of 100  $\mu\text{m}$  (Supplemental Fig. 2J). To show how disorganized the initial set of vectors within the zone of averaging was, we plotted the standard deviation of the set as a color code. For statistical comparison of embryos, certain areas were selected in the caudal heart and on both sides of the future omphalomesenteric veins. Velocity vectors from different embryos, but within the same location, were pooled. Data obtained from different embryos were considered statistically independent.

## Results

### *The structure of early cardiac ECM*

We collected quail embryos at stages ranging from HH8–, when endothelial and endocardial progenitors first demonstrated a strong QH1 immunoreactivity, to HH11. Whole-mount embryos were immunolabeled for QH1 and selected ECM components, fibronectin and fibrillin-2, and the anterior embryonic tissues were subjected to confocal microscopy. At HH8–, ECM fibrils were already abundant in the vicinity of QH1-positive endothelial/endocardial progenitors (Figs. 1A, A'), however for later stages we noted an increasing degree of association between fibronectin and vascular progenitors. By HH10, the forming cardiac tube and omphalomesenteric veins were surrounded by a fibronectin “sheath” (red arrows in Figs. 1B', C').

Fibrillin-2 was organized in coarser structures than fibronectin. Fibrillin-2 fibrils also indicated a certain degree of association with the membranes of endothelial/endocardial progenitors. At HH10 and 11 fibrillin-2 was detected only on the endocardial side of the cardiac jelly (red arrows in Fig. 1D'), whereas fibronectin was present on both the myocardial (blue arrow in Fig. 1D') and endocardial sides of the cardiac tube ECM. At the stages investigated, both ECM components were interspersed, but did not colocalize to identical filamentous structures.

### *ECM from the caudal embryo contributes to the caudal heart tube*

Fibronectin and fibrillin-2 were immunolabeled *in vivo* with distinct fluorophores in live, HH7 quail embryos ( $n=9$ ). The specimens were recorded in time-lapse between stage HH8– and HH12. The displacements of individual ECM fibrils were followed using a manual tracking procedure. ECM structures preserved recognizable features during the transition from their initial, lateral positions in the precardiac mesoderm to their inclusion into the cardiac tube ECM at HH10. The large ECM density within the forming heart tube precludes filament tracking at later stages of development. Fig. 2 and Movie S1 demonstrate that both fibronectin and fibrillin-2 fibrils are engaged first in a centripetal, then in a midline-directed movement. Adjacent trajectories are very similar, regardless of the molecular identity of the tracked ECM component.

By extensive ECM tracing, the anatomical origin of ECM filaments that contribute to the developing heart tube was determined in HH8 embryos. We analyzed  $n=3$  embryos in which both ECM

constituents were labeled. Tracking was performed independently for each ECM component. The obtained trajectories were assigned four groups depending on the filament's fate at HH10 (Movie S2).

By superimposing the four groups on DIC image sequences, the approximate boundaries were identified for each category of markers (Fig. 2B). The resulting ECM positional fate maps were similar for each embryo analyzed as well as for both fibronectin and fibrillin-2. We consistently found that ECM flanking the AIP at HH8– contributed to the anterior one third of the heart tube at HH10 (the red area in Fig. 2B). Bilateral areas located laterally to the caudal segments of the “red” or cranial ECM zone (denoted as yellow areas in Fig. 2B) are the source of ECM fibrils that were translocated to the middle portion of the cardiac tube by HH10. The regions contributing ECM to the caudal heart tube and omphalomesenteric veins maps to the posterior ends of the AIP and caudally extends to the level of the second or third somite pair (green areas in Fig. 2B). The lateral borders of this caudal-most region closely approach the boundary of the area opaca.

### *ECM from the cranial embryo is incorporated into the growing heart tube from the cranial end*

Upon initial assembly at HH10, the heart tube undergoes rapid elongation of all three contributing layers (endocardium, cardiac jelly and myocardium), concomitant with the onset of looping (Fig. 3B). We followed immunolabeled individual ECM fibrils on the ventral surface of the foregut, in the vicinity of the tubular heart. These fibrils are included in the ECM layer separating the foregut endoderm and ventrally-positioned splanchnic mesoderm (Fig. 3A). Between HH10 and early HH11 a number of ECM fibrils were displaced toward the ventral midline with subsequent inclusion into the anterior pole of the elongating cardiac tube and dorsal mesocardium (Fig. 3B, Movie S3). Due to dramatic changes in morphology of the anterior embryo that occur between HH7 and HH10, we could not reliably trace the earlier (prior to HH10) origins of these filaments.

### *Exogenous fibronectin participates in tissue movement and incorporates into the heart tube along with the endogenous precardiac mesoderm ECM*

To show that tagged ECM filaments, suitably located in the anterior LPM, indeed incorporate in the cardiac jelly, we performed experiments utilizing exogenous, fluorescently-conjugated human serum fibronectin (BD Biosciences). 7–10 ng of either AlexaFluor647 or 555 fluorophore-labeled fibronectin was delivered subendodermally into the LPM of quail embryos at HH6–8 ( $n=6$ ). The endogenous fibronectin network of these embryos was also immunolabeled. Recordings of subsequent embryonic development revealed that the exogenously-added human fibronectin incorporated into the quail ECM network and participated in its displacements in a manner indistinguishable from endogenous fibronectin molecules (Supplemental Fig. 3 and Movie S5).

As a control, we delivered 100–150 ng of BSA conjugated to AlexaFluor 647 to the contralateral side of each embryo. Time-lapse recordings demonstrated that the BSA signal completely dissipated within 4 h after injection, whereas the exogenously-added fibronectin signal was detectable for up to 12 h. Furthermore, the distribution of fluorescent BSA was devoid of any fibril-like patterns throughout the experiment.

To determine the position-fates of exogenously-added fibronectin in the LPM, 25–30 ng of fluorescently-conjugated fibronectin was microinjected into 6–10 adjacent sites along the LPM of HH7–8 embryos ( $n=12$ ). Injections were performed in such a way that medial (paraxial) and lateral (precardiac) portions of the anterior mesoderm were targeted with differentially-labeled fibronectin molecules (Fig. 4A, top panel). Time-lapse imaging was used to record

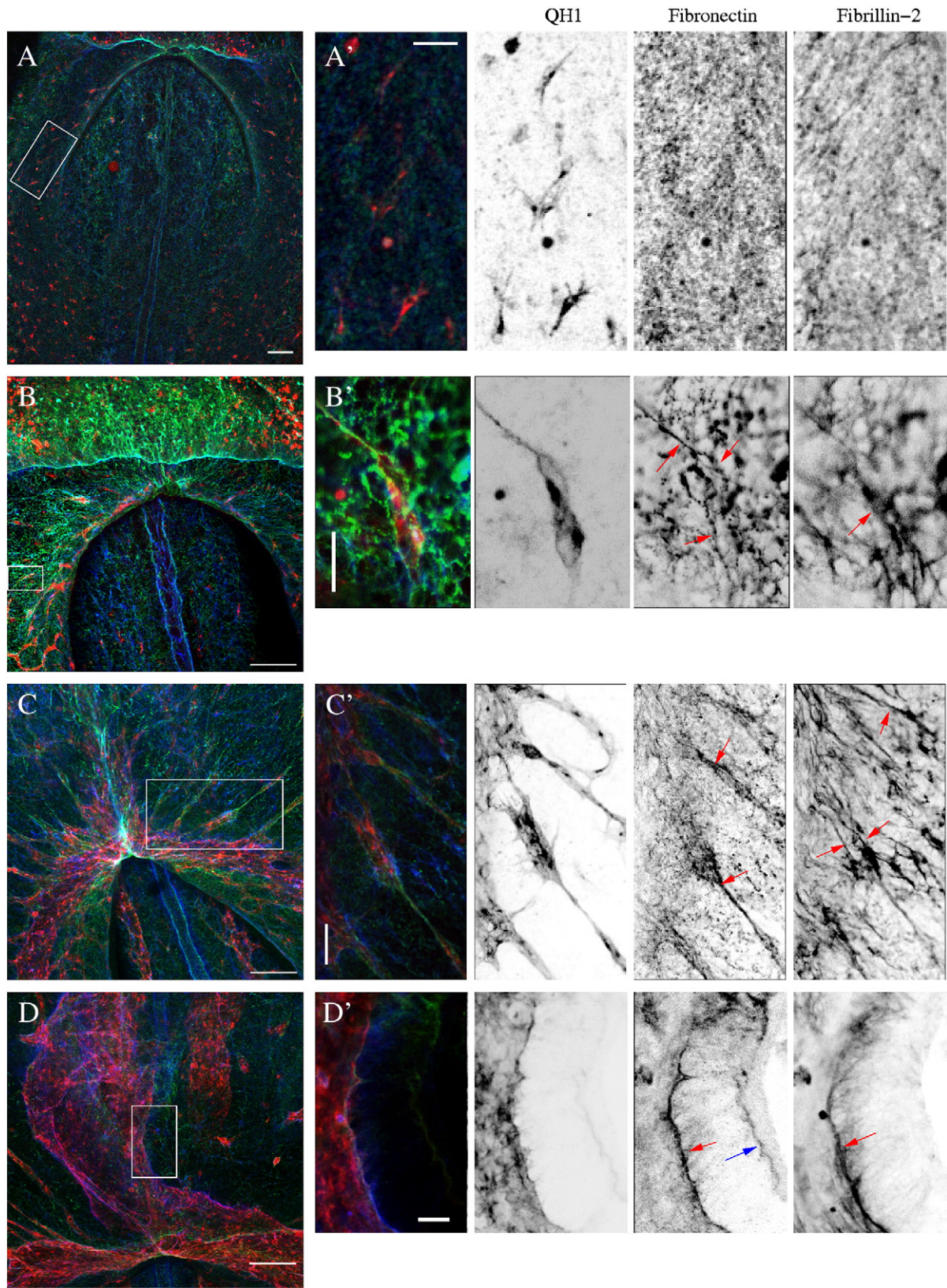


**Fig. 1.** Endocardial tube assembly takes place in a microenvironment abundant in fibronectin and fibrillin-2 ECM. A–D: maximum intensity dorso-ventral projections of confocal stacks obtained at HH8 – (A), HH8 (B), HH10 (C), HH11 (D) stages of development. Whole mount specimens were immunostained with monoclonal antibodies QH1 (red), B3D6 anti-fibronectin (green), and JB3 anti-fibrillin-2 (blue). A'–D': single, 2.5–4  $\mu\text{m}$  thick optical plane images selected from the regions marked with rectangles in panels A–D. In addition to the multicolor merged image, distinct panels show each immunofluorescence label inverted for better contrast. Scale bars: A–D—100  $\mu\text{m}$ , A', C'—40  $\mu\text{m}$ , B', D'—20  $\mu\text{m}$ . Fibronectin fibrils demonstrate an increasing degree of association with endocardial cell surfaces at progressively later developmental stages (red arrows). Fibronectin is also associated with the myocardium at HH11 (blue arrow). Fibrillin-2 fibrils are somewhat larger in diameter and appear to be aligned with the QH1-positive cell surfaces (A–C, A'–C', red arrows). Both types of ECM surround the endocardial layer in the assembled heart tube (D, D').

the rearrangements of exogenously-added fibronectin occurring between HH8 – and 11 (Movie S6). Beginning at stage HH8, ECM aggregates derived from the laterally-positioned human fibronectin pool are seen to move toward the ventral midline, where fibrils eventually become incorporated in the tubular heart (arrowheads in Fig. 4A).

In transverse cryosections of the heart tube we compared the distribution of endogenous and exogenously-added fibronectin (Fig. 4). The former was detected by immunostaining sections with monoclonal anti-fibronectin antibody, B3D6. In each embryo sectioned following the time-lapse acquisition ( $n = 5$ ), exogenously-added fibronectin was found exclusively on the endocardial side of

the cardiac jelly (i.e., the basal side of the endocardium). In embryos fixed at HH10 ( $n = 2$ ; data not shown), exogenous fibronectin, delivered to the caudal embryo, was found on the basal side of the endocardium, throughout the length of the cardiac tube. This is consistent with our tracking results (Fig. 2; Movie S1), suggesting that (endogenous) fibronectin derived from the caudal embryo gives rise to ECM of the early heart tube (at HH10). At the same time, in embryos fixed at HH11–12 (Fig. 4) caudally-derived exogenous fibronectin was mostly found associated with the endocardium in the caudal half of the heart ( $n = 3$ ).

However, if a 10-fold greater amount (200–250 ng) of exogenous fibronectin was delivered to the LPM at HH7, the fluorescent molecule was also found in small amounts on the myocardial side of the cardiac jelly throughout the length of the heart tube, in embryos fixed at HH11 (Supplemental Fig. 4). In contrast, no contribution to the cardiac jelly was detected from the medially-positioned exogenous fibronectin (green in Fig. 4A) either by time-lapse imaging of live embryos or in transverse sections of fixed tissue (data not shown).

#### *Early endocardial development, visualized by TIE1 promoter activity*

The TIE1 promoter is active in endothelial cell progenitors beginning at late HH6 (Sato et al., 2010). Thus, the TIE1:H2B-YFP transgenic embryos offer a novel way to study the movements of future endocardial cells throughout heart development. To analyze the developmental stage-dependent movements of future cardiac ECM and endocardial cells, we identified seven characteristic morphological states of the anterior embryo that we further refer to as endocardial stages, ES1–7 (Supplemental Fig. 5). These stages represent a 14–16 h interval from HH8 – to 11. During this time the nascent endocardium undergoes a dramatic transition from a predominantly single-cell progenitor organization to a tubular, lumenized tissue. Our classification scheme is based on the apparent changes in (TIE1+) endocardial organization, and stands in contrast to the standard HH classification of avian embryonic development. Classification of HH stages 7–14 is primarily based on the somite pair number (Bellairs and Osmond, 2005; Hamburger and Hamilton, 1951). However, addition of new somites and progression of endocardial morphogenesis are not always precisely temporally correlated.

At ES1–3 endothelial/endocardial progenitors are flanking the AIP; at this stage the apparent linear distance between the caudal border of the headfold and the posterior margin of the anterior intestinal portal is minimal, with few Tie1::H2B-YFP+ endocardial progenitors seen at the ventral midline. Although the foregut and the heart tube are at different dorsal/ventral planes, we used an increase in the projected distance between the two anatomical landmarks (viewed ventrally) as the index of foregut regression and midline mesoderm fusion. Both the headfold-to-AIP index (distance) and the number of Tie1::H2B-YFP+ progenitors progressively increased during ES2 and 3.

The ES4 stage was typified by an elongated plexus of Tie1::H2B-YFP+ pre-endocardial cells assembled at the ventral midline, i.e., the nascent endocardial tube. Also, at ES4, aggregations of endothelial/endocardial progenitors mark the sites of the omphalomesenteric veins, which form anterior and ventral to the AIP. By ES5 the

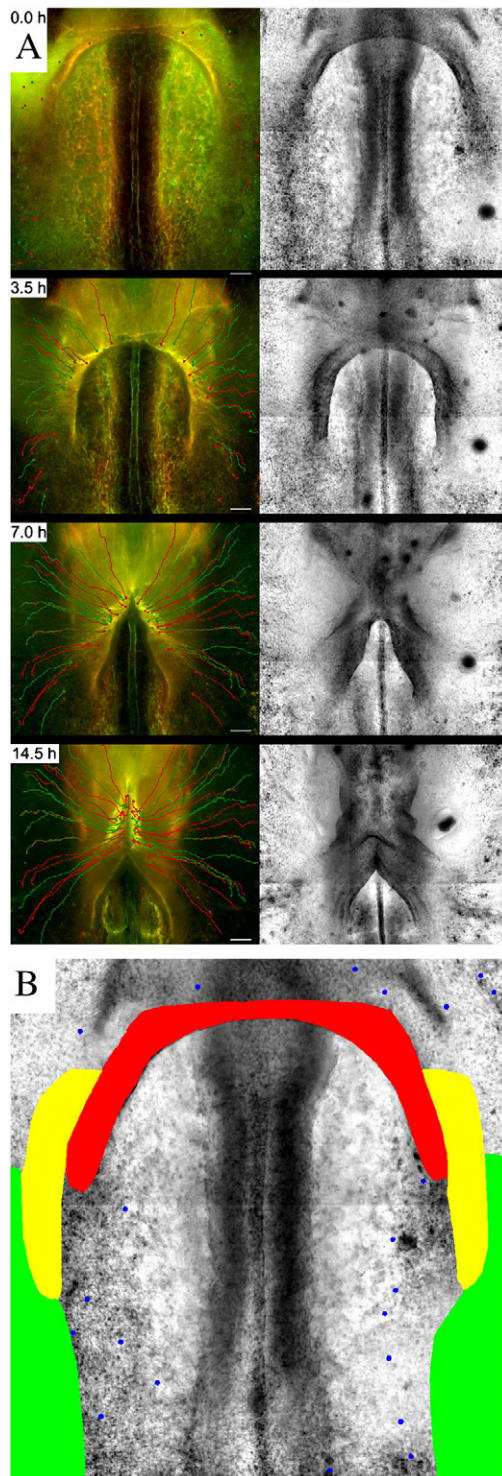


**Fig. 2.** Fibronectin (red) and fibrillin-2 (green) fibrils derived from the LPM at HH8 – translocate to the heart by HH10. A: Corresponding epifluorescence (left) and DIC (right) image pairs, representing development between HH8 – and HH10. ECM movements are indicated by the superimposed trajectories. Scale bars—100  $\mu$ m. B: Schematic fate map of ECM fibrils in a HH8 – stage embryo. ECM from the colored areas incorporates into the cranial (red) or middle (yellow) portions of the heart tube, or to the caudal heart tube and the omphalomesenteric veins (green) by HH10. Blue dots indicate ECM fibrils that do not incorporate into the heart. The fate map shown is a representative example out of 3 specimens that were imaged and analyzed by identical methods. See Movies S1 and S2.

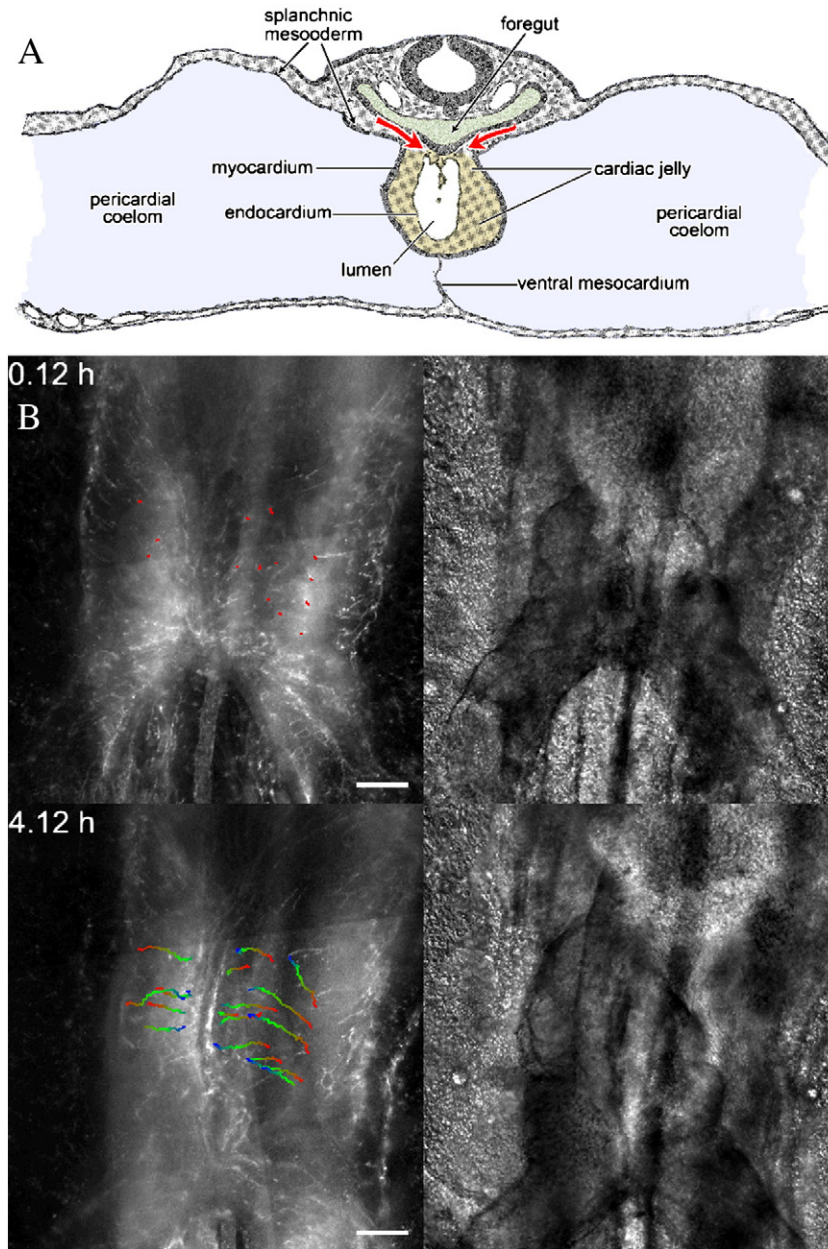


**Fig. 3.** ECM positioned ventral to the pharyngeal endoderm is translocated toward the anterior portion of the tubular heart and contributes to its elongation after HH10. A: Schematic transverse section, adopted from Lillie, 1930. B: Corresponding fibrillin-2 immunofluorescence (left) and DIC (right) image pairs are shown. During the elapsed 4 h, the length of the cardiac tube substantially increases (DIC panels). Superimposed trajectories of individual fibrils are color-coded: red, green and blue colors indicate progressively later trajectory segments. The movements of fibrillin-2 fibrils are indicated by the red arrows in panel A. Scale bar—100  $\mu$ m.

developing endocardial plexus/tube has nearly doubled in length. Nascent omphalomesenteric veins incorporate an increasing number of cells at subsequent stages (ES5–7), with the concomitant organization of endothelial cells into tubes. Subsequently, individual small-caliber endocardial tubes fuse to form a single lumenized tube (confirming the findings of Drake et al., 2006). We ranked embryos with linear heart tubes displaying a slight asymmetry to the right as ES6, while “C-shaped” hearts are defined as ES7. With respect to the HH classification, ES1 corresponds to HH8–, ES2–4 to HH8–8+, ES5 to HH9, ES6 to HH10, and ES7 to early HH11.

#### *Tissue movements visualized by ECM displacements*

Quantitative characterization of ECM movements during early heart development was performed using epifluorescence recordings

of 6 embryos, each microinjected with fluorophore-conjugated antibodies labeling fibronectin and fibrillin-2. Image pairs that correspond to the various endocardial stages (ES) were subjected to PIV analysis. In-plane (two-dimensional) ECM displacements were measured in each deconvolved focal plane by independent computations. The velocity data are presented in a reference system co-moving with the somitic mesoderm. This procedure allows us to establish the typical “local” ECM movements characteristic for each stage of the heart development process as well as to compare movements of fibronectin to those of fibrillin-2.

Fig. 5 shows the pattern and distribution of fibronectin and fibrillin-2, as well as a typical velocity snapshot of their movements in an early (ES1, panel A) and later (ES7, panel B) stage of heart development. In the early stages, the ECM moves centripetally, quite uniformly along the posterior margin of the AIP. In later stages,

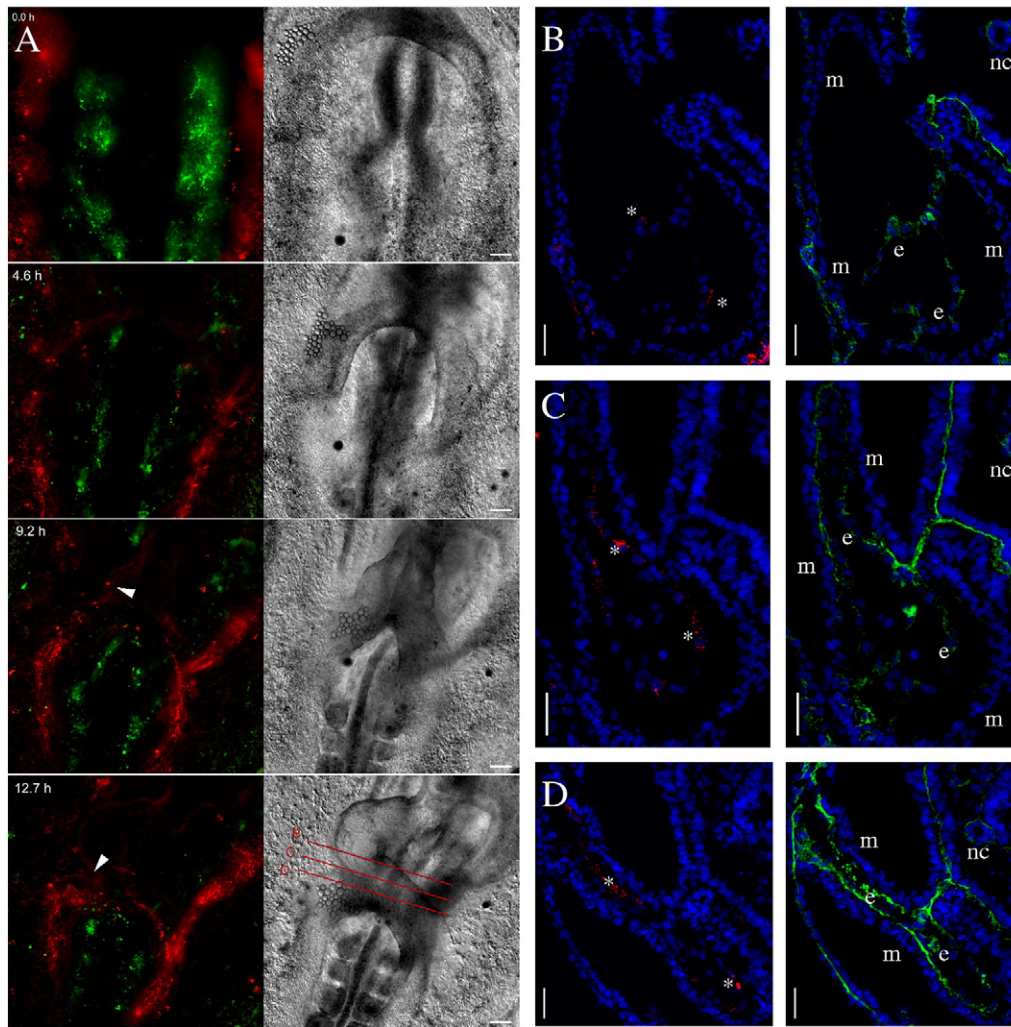


**Fig. 4.** Exogenous fibronectin, injected into the LPM, incorporates into the cardiac tube. Human fibronectin conjugated to Alexa555 (red) was injected into the anterior LPM at HH7, while fibronectin-Alexa647 (green) was delivered to the paraxial mesoderm and medial-most regions of the LPM. **A:** Corresponding epifluorescence (left) and DIC (right) image pairs, showing an embryo at HH8 – (top), HH8+, HH10, and HH11 (bottom) stages of development. Some fibronectin fibrils derived from the lateral (red) pool are progressively displaced toward the forming heart tube, which begins to exhibit Alexa555 fluorescence at HH10 and 11 (white arrowheads). At the same time, a large portion of the laterally-injected fibronectin pool remains associated with mesodermal and endodermal tissues in the anterior embryo. The medially-delivered (green) fibronectin pool does not contribute to the cardiac jelly. Scale bars—100 μm. **B–D:** Transverse cryosections through the heart tube of the same embryo shown in panel A, fixed at HH 11. Approximate planes of section are indicated in the bottom right frame of panel A. Red fluorescence signal corresponds to the exogenous fibronectin-Alexa555. The green signal shows the distribution of endogenous quail fibronectin, labeled with B3D6 antibody post-sectioning. DAPI staining of cell nuclei is shown in blue. Human fibronectin is present at the endocardial-cardiac jelly interface (asterisks). nc: notochord, e: endocardium, m: myocardium. Scale bars—40 μm.

movements diminish at the anterior aspect of the forming heart, while the posterior aspect of the heart continues its centripetal, medio-posterior expansion.

We compared ECM displacement speeds at three distinct reference points: one located at the most anterior, and two at the left and right portions of the AIP “arch” (Figs. 5A and B). An ANOVA analysis comparing the velocity magnitudes at the three locations failed to reveal statistically significant differences at any of the seven endocardial stages investigated ( $p > 0.5$ ). Thus, we consider the centripetal contraction of the posterior margin of the foregut (endodermal tissue) uniform along the whole posterior margin. The speed of centripetal expansion is fastest at ES2 (around 70 μm/h) and drops continuously afterwards (Fig. 5C).

At each grid point of the PIV calculation, we can calculate the difference between the displacement vectors characterizing the two ECM components. Except for the first stage (ES1), the mean magnitude of the calculated difference is less than 10% of the magnitude of the total tissue displacement, and this difference may reflect systematic errors in our PIV analysis. Thus, while fibronectin and

fibrillin-2 do not co-localize in the same filaments, their tissue-scale displacements are virtually identical at each stage of the transition from planar precardiac mesoderm to formation of the heart tube. Therefore, either fibrillin-2 or fibronectin can be used as a reporter for tissue-scale movements.

#### *Movement of endocardial and endothelial progenitors*

To characterize the motile behavior of endocardial and endothelial cells, Tie1::H2B-YFP nuclei were traced in consecutive image stacks both manually and by using the automatic tracker program CIPA. As Fig. 6 and Movie S8 demonstrate, endocardial and endothelial progenitors may be located near one another at HH8, but then the two groups progressively separate as the endocardial progenitors, located within a horseshoe-shaped field, begin their centripetal movement toward the embryonic midline. The boundary, which separates future endocardial cells from endothelial cells, is quite sharp (Fig. 6A, right panel). Furthermore, the anatomical origin of

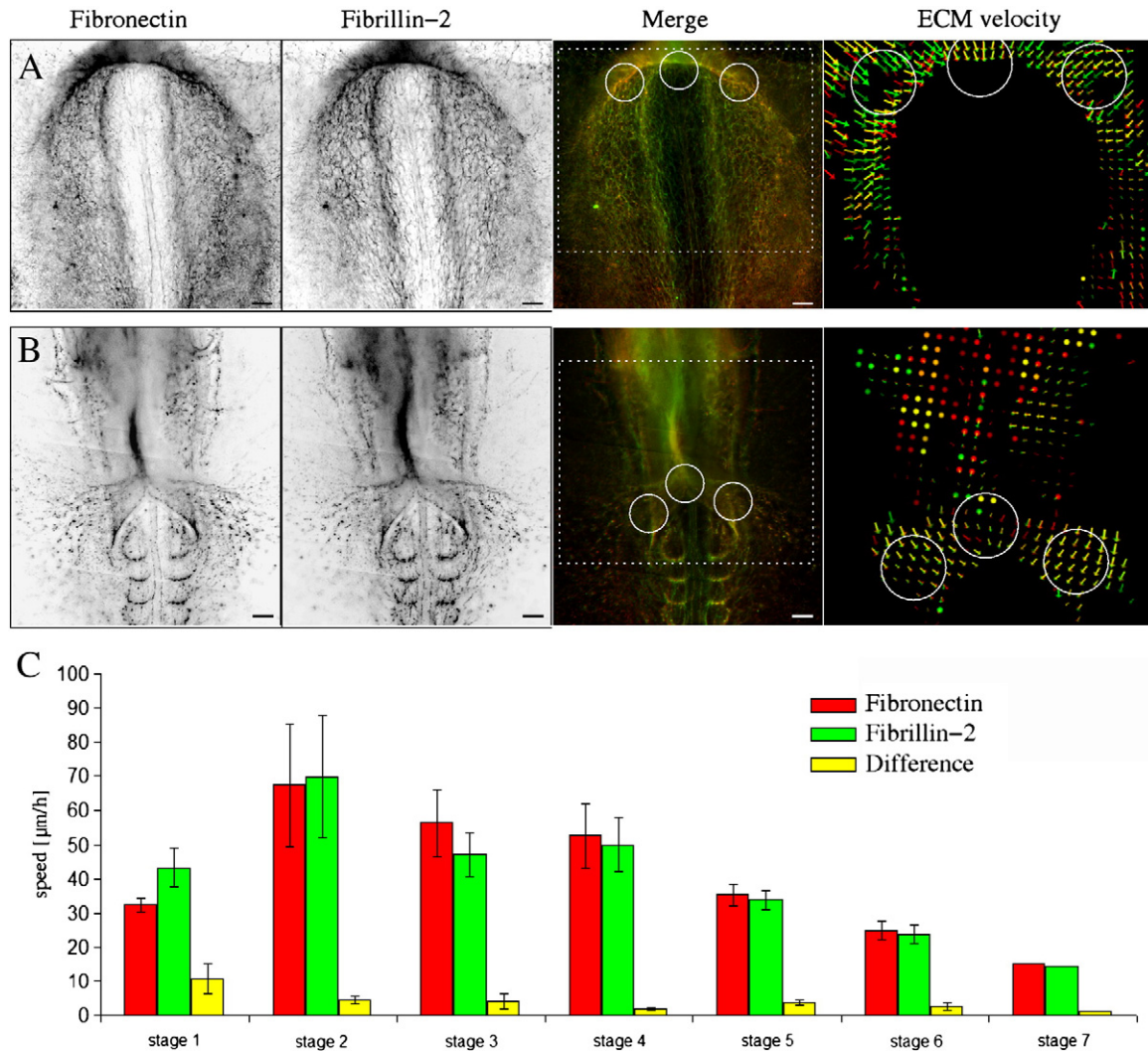


**Fig. 5.** Large-scale displacements of fibronectin and fibrillin-2 structures are identical. A, B: Fibronectin and fibrillin-2 immunostaining (inverted for better contrast) and their superimposed images (third column) are shown together with the corresponding PIV velocity vector map (fourth column). The embryos shown represent an early (ES1, panel A) and a later (ES7, panel B) stage of development. The velocity fields show fibronectin (red vectors) and fibrillin-2 (green vectors) movements in a selected frontal optical plane intersecting the forming heart. Vectors represent velocities as extrapolated displacements during one hour. The reliability of the vectors is indicated by color brightness. Overlap between the two colors appears as yellow. Dots indicate the absence of movement, i.e., velocities smaller than 10  $\mu\text{m}/\text{h}$ . Scale bars—100  $\mu\text{m}$ . C: Mean speed of centripetal ECM movements along the AIP and the inflow region, measured within locations similar to the indicated circles in panels A and B. For each endocardial stage of development, the average speed of ECM displacements is shown for both fibronectin (red) and fibrillin-2 (green). The average magnitude of the difference between the two is presented in yellow. Error bars indicate SEM; distinct specimens were considered statistically independent.

the cardiac jelly ECM (Fig. 1B) closely corresponds to that of the endocardial progenitors.

Representative recordings of Tie1:H2B-YFP embryos, which were also microinjected with fluorophore-labeled ECM antibodies, were analyzed by manually tracking TIE1 + nuclei and ECM filaments. As Fig. 6B and Movie S7 reveal, cell and ECM trajectories are surprisingly similar. This degree of similarity suggests that the active motility of future endocardial cells is small relative to the local ECM environment. To estimate active cell motility, at each recorded time point we subtracted the average displacement of nearby-traced ECM filaments from the observed cell displacements. As Fig. 6C and D demonstrates, the trajectories of active cell movements (red) are random, with little persistence compared to the trajectories of total cell displacements (green) corresponding to Fig. 6B.

At HH9–10 the endothelial/endocardial progenitors form a vascular plexus (DeRuiter et al., 1993), associated with splanchnic mesoderm ventral to the foregut. Cells constituting this plexus engage in a midline-directed movement commencing at HH10 and continuing until at least HH12 (Supplemental Fig. 6 and Movie S4).

This movement also correlates in location and timing with the medial-ward ECM motion seen in Fig. 3 and Movie S3.

To characterize better the active movement of Tie1 + cells, we selected on average six, but at least four, embryos at each stage of heart development (ES1–7). We determined the local ECM movements by PIV analysis; YFP-expressing nuclei were tracked either by the automatic CIPA tracker (raw data not shown) or by PIV analysis (Supplemental Fig. 5, panel three). Active cell movements (Supplemental Fig. 5, panel four) were established as the difference between the local (PIV- or CIPA-estimated) cell-based and ECM displacement vectors. This analysis reveals that while the total cell displacements (just like the ECM movements) are centripetal (Supplemental Fig. 5, ES3), active cell movements have a medially-directed bias in the medial-most regions of the omphalomesenteric veins (Supplemental Fig. 5, ES5), while in the more lateral aspects of these veins, such a medial bias is not observed.

Cellular movement speeds, averaged from multiple specimens, are shown in Fig. 7C. As expected, due to the local averaging, values obtained by PIV are somewhat smaller than the values obtained by

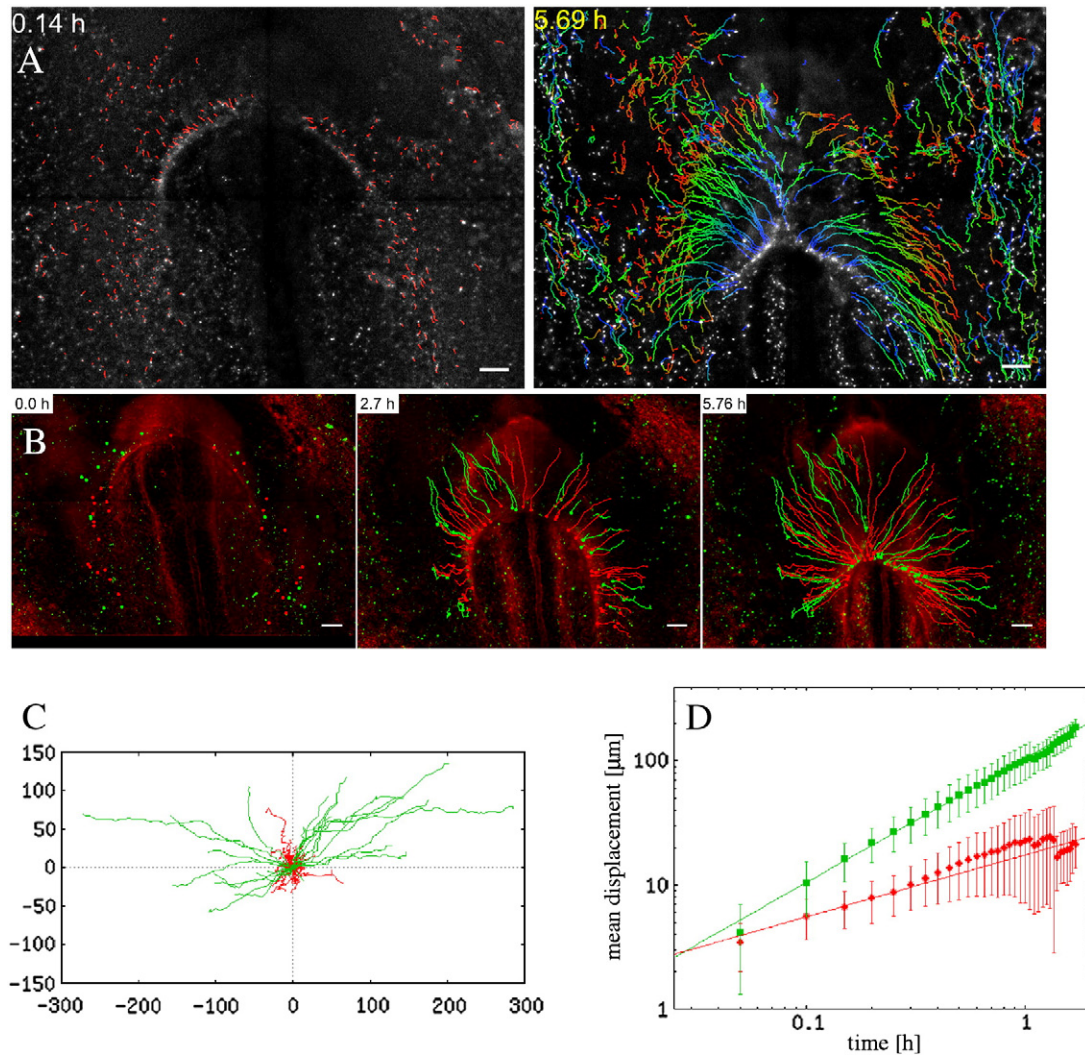


**Fig. 6.** TIE1 + endocardial progenitors are spatially segregated from the endothelial population and participate in coordinated midline-directed displacement along with the ECM in the adjacent tissue. **A:** Epifluorescent images of a Tie1::H2B-YFP transgenic embryo at early (HH8, left) and later (HH9, right) stages of development, with superimposed trajectories of endothelial and endocardial progenitors. Cell trajectories were obtained using the CIPA automated tracking software; the color-code conveys timing information as in Fig. 3. Scale bars—100 μm. **B:** Trajectories of manually-traced Tie1::H2B-YFP pre-endocardial cells (green) are compared with those of fibrillin-2 filaments (red). **C:** Trajectories representing the total (green) and active (red) movements of tracked pre-endocardial cells. Trajectories shown in panel C are re-plotted in such a way that each cell starts from the origin (green trajectories). Active cell movements (red trajectories) were estimated by subtracting the local ECM movements from the total displacements. **D:** Mean displacement vs. elapsed time for the total (green symbols) and active (red symbols) cell movements. On a double logarithmic plot a line with slope 1 (green line) indicates persistent motion (displacement and elapsed time are proportional), while a line with slope 1/2 (red line) indicates random walk (displacement is proportional to sqrt(t)). Error bars represent standard deviation, obtained from a pool of all tracked cells.

the CIPA tracker, and both are higher than the values obtained for ECM displacements. The average speed of active cell movement decreases slightly from 20 μm/h to 15 μm/h between the early and later stages of heart development. The calculated mean speed of the lateral drift is  $7 \pm 2$  μm/h; thus fluctuations in cell speed are substantial, which is in agreement with the random walk-like trajectories calculated in Fig. 6D (red plots).

#### *Tissue movements are able to convect passive objects*

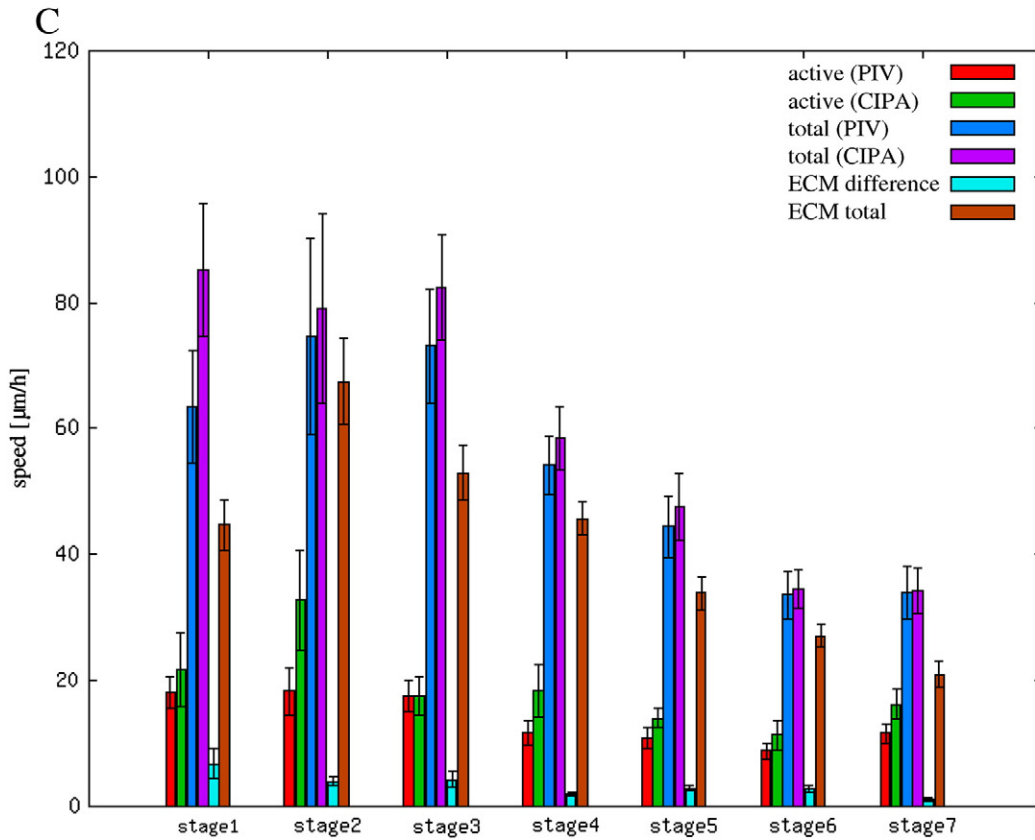
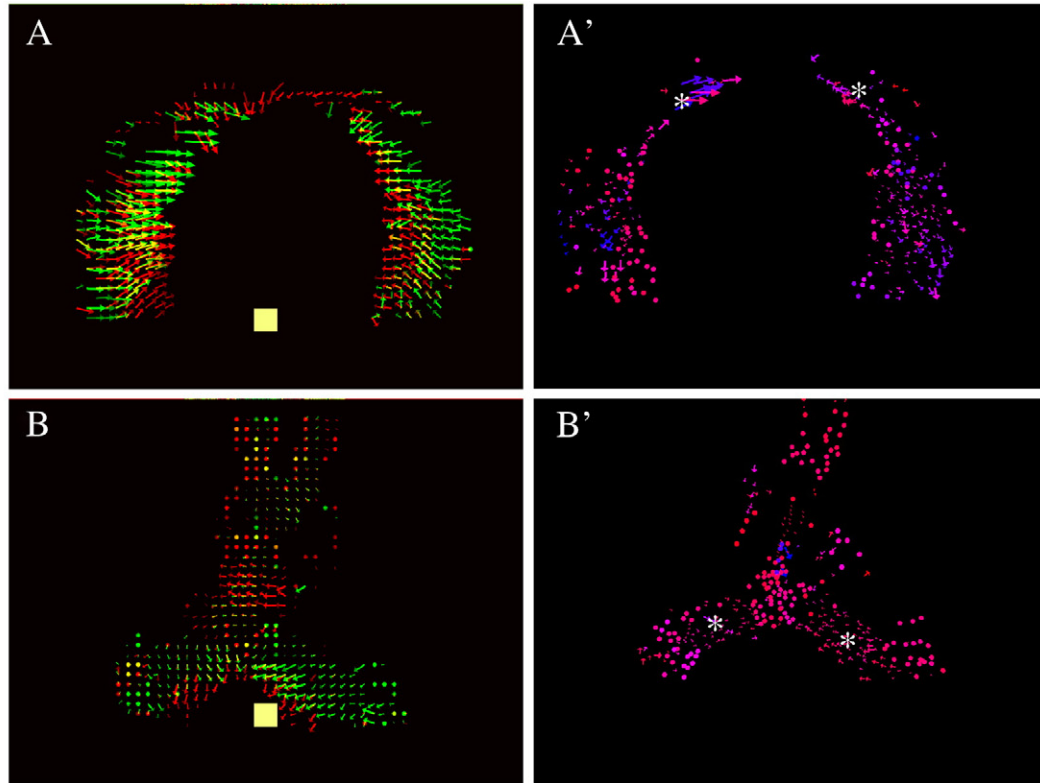
To give further support to the idea that minimal autonomous directed motion is required from the endocardial cells to construct the heart, we tested whether passive objects placed in the vicinity of the precardiac mesoderm are transferred to the heart tube by means of global tissue flow. We performed the experiments using embryos

**Fig. 7.** Active and total movements of Tie1::H2B-YFP pre-endocardial cells. **A** representative specimen is shown at an early (panels A and A', ES 1) and a later (panels B and B', ES 7) stage of heart development. Images in panels A and B show velocity vectors (red for ECM and green for cells) in a selected frontal optical plane intersecting the forming heart. Velocities are indicated as extrapolated displacements over a 1 h long time period, the yellow square indicates a linear size of 100 μm. The reliability of the vectors is estimated by the contrast of the local fluorescence, and indicated as color brightness. The locally prevalent direction and speed of active cell movements was determined by averaging the vectors of active cell velocities within a radius of 100 μm. These vectors, projected to a frontal plane, are shown in A' and B', and thus represent the local directional bias of active cell movements. The color assigned to the vectors indicates the local standard deviation of active cell movements: blue and red colors indicate locally ordered (small standard deviation—vectors pointing in similar directions) and disordered movements, respectively. Notice the tendency to move toward the heart in the vicinity of the forming heart tube (asterisks). **C:** Speeds of active (bars 1 and 2) and total (bars 3 and 4) cell movements, the corresponding speed of ECM displacements (bar 6), and for comparison the calculated difference in the movements of the two ECM components (bar 5) are shown for the seven stages of endocardial development (See Supplemental Fig. 5). Cell displacements are estimated by two methods, PIV (bars 1 and 3) and automated cell tracking (bars 2 and 4), and yield similar results.

( $n = 3$ ) in which fibrillin-2 was immunolabeled at HH7–8 – (right before or at ES1). Subsequently, latex beads, 6.5  $\mu\text{m}$ , were placed under the endoderm by a series of microinjections. Delivery of the beads was targeted to the regions that correspond to the position of precardiac mesoderm at HH7 as defined in recent fate mapping studies (Cui et al., 2009; Abu-Issa and Kirby, 2008). Time-lapse imaging commenced at

HH8 (ES1–2) and continued until HH11–12 (ES7 and beyond). For analysis, we selected the groups of beads that moved toward the ventral midline and incorporated into the heart tube (based on subsequent confocal analysis).

Beads placed caudal to the AIP entered the heart tube from the inflow end (e.g. the group of beads indicated with an (a) in Fig. 8). Beads



positioned ventrally to the foregut at HH8 [groups marked with (b) and (c) in Fig. 8] were incorporated into the forming heart tube from its anterior (outflow) pole (Movie S9). Both outcomes correlate with the position-fates of the ECM in corresponding areas (Figs. 2 and 3). Moreover, PIV analysis of bead velocities results in similar values to those of adjacent fibrillin-2 ECM (data not shown). The calculated difference between the displacement vectors of the two components is less than 10% of the magnitude of total tissue displacements: a finding that also serves as a negative control for our active motility calculations.

## Discussion

### *The source of early cardiac ECM*

At early stages, components of the primitive heart ECM (including ECM associated with the heart splanchnic mesoderm and endoderm) include collagens I, IV, fibrillins –1 and –2, fibronectin, and laminin (Drake et al., 1990). It is believed that many of these components persist and contribute to the cardiac jelly at tubular heart stages (reviewed in Little and Rongish, 1995).

The current understanding of cardiac jelly formation between the myocardium and endocardium relies on the biochemical studies of Krug et al. (1985). As the endocardial and myocardial tubes are fusing at the ventral midline, the myocardium secretes a thick acellular matrix that helps to separate the two cell layers of the heart. The cardiac jelly exists as the fusion between this larger myocardially-derived BM (having a lamina densa and an extended reticular lamina) and an attenuated, endothelial-associated BM (composed only of a lamina densa), but is not itself organized as a basement membrane-like structure (Kitten et al., 1987).

The myocardium, however, does not secrete all components of the cardiac ECM. In rat embryos the mesoderm actively expresses fibronectin at the early primitive streak stages, but then this expression ceases at the pre-headfold stage. Fibronectin expression is resumed by endocardial cells in the early heart tube at the 5-somite stage (Suzuki et al., 1995), which morphologically corresponds to HH8 + in avians. The endocardium continues to actively express fibronectin until the 14-somite (HH11 stage). In contrast, myocardial cells do not express fibronectin at any of these early stages of development. Thus, the endocardium is believed to be the main source of fibronectin in the cardiac jelly.

In addition to ECM components produced “de novo”, in this work we demonstrate that fibronectin and fibrillin-2 filaments (both endogenous and exogenously-added), which are associated with the LPM at HH8, become incorporated into the cardiac jelly by HH11. The ratio of the transported and newly-synthesized ECM is difficult to estimate. Our time-lapse recordings as well as confocal microscopy studies indicate that the incorporated, endogenous, labeled ECM is abundant enough to form an ECM-dense layer that is continuous at the resolution of optical microscopy.

### *ECM movements*

This work represents the first demonstration of ECM filaments being translocated and incorporated into a future organ. Our group has previously shown that fibrillin or fibronectin-containing ECM fibrils are convected during primitive streak formation and gastrulation (Zamir et al., 2006, 2008) and vertebrate axis formation (Czirók et al., 2004). Further, recent work by others showed fibronectin fibrils are translocated in the presomitic mesoderm during avian axis elongation (Bénazéraf et al., 2010).

Like cardiac precursor cells, ECM filaments are displaced and enter into the forming heart tube at both the anterior and posterior regions (See Movie S1). The ECM is added to the elongating heart tube concomitantly with the addition of cardiac segments. The area of the LPM that contributes ECM to the forming heart closely corresponds

to the fate map of myocardial precursors (Cui et al., 2009) and our data on endocardial precursor cell origin (See Fig. 6). Like the cells contributing to the primary heart field, the ECM fibrils come from specified regions of the embryo and maintain their anterior–posterior relationships to one another (Fig. 2 and Movie S2). Thus, both cellular and ECM fate maps have three somewhat overlapping regions which distribute to different portions of the heart along the anterior–posterior axis. The ECM and cells contributing to the anterior portion of the stage 10 heart tube were observed in the anterior-most “arch” spanning the embryonic midline (Figs. 2 and 6).

### *ECM movements and morphogen gradients*

The maintenance of anterior–posterior positional order during the time the cardiac jelly (fibronectin and fibrillin-2) is accumulated (Fig. 2) has implications for the establishment/maintenance of ECM-bound morphogen gradients. If gradients of morphogens are “pre-established” outside of the forming heart tube, and if the ECM-bound morphogens are then swept into the heart with the same relative positions, a corresponding anterior–posterior morphogen gradient may be maintained. Similarly, any left/right asymmetry in the distribution of ECM molecules/bound morphogens in the lateral plate would likely be maintained in the heart tube.

Although we have no direct evidence that fibronectin and/or fibrillin-2 are binding morphogens key to heart morphogenesis, other studies have shown that fibronectin controls the availability of growth factors such as TGF $\beta$  (Fontana et al., 2005; Leiss et al., 2008), and can bind VEGF (Wijelath et al., 2002), in some cases acting in a synergistic manner with heparan sulfate (Stenzel et al., 2011). In addition, although this study focused on the movements of fibronectin and fibrillin-2, we propose that other ECM components (including those that bind morphogens) likewise are displaced as part of an interconnected ECM scaffold; indeed it is difficult to argue that the ECM does not move as a composite material.

In general terms, the cells closest to a source of a given morphogen are believed to be exposed to a higher concentration gradient of that morphogen. Thus, endocardial cells moving with their nearby ECM (and any ECM bound morphogens) toward the midline have the potential to be exposed to a relatively “static” morphogen level, provided the morphogen bioavailability also remains constant. The degree to which cells are sensitive to the ECM-bound morphogens is influenced by numerous factors, including: 1) the rate of morphogen accumulation, 2) the time between morphogen secretion and binding to the ECM, 3) the length of time a given morphogen remains bound to the ECM, 4) the spatiotemporal activity of potential proteolytic enzymes, 5) the “half-life” of the morphogen in solution, 6) the location of binding partners/receptors and 7) the morphogen diffusion rate (Drocco et al., 2011; Yu et al., 2009). Thus, although potential target cells and ECM-bound morphogens move together, it is entirely possible that the displacements of the ECM could have little bearing on the morphogen gradient. If a morphogen is secreted by a cell and is quickly bound to nearby ECM, and if that morphogen remains bound for only a short period of time, then the movement of the ECM is not a major influence on the repositioning of the morphogen (i.e. the morphogen is not “carried” by the ECM any substantial distance).

The fact remains that the ECM is highly dynamic, and that at the tissue-level scale, its movements are predictable and reproducible (Fig. 2). These empirical data indicate the need to study cell signaling within the context of a physiologically relevant, highly dynamic ECM environment.

### *The source of endocardial cells*

Cardiac progenitors are among the first cell populations to undergo ingress through the primitive streak, which in turn is followed

by their rapid anterior and lateral movements. Subsequently, cardiac progenitor cells, i.e. those cells that will reside in the midline heart tube by HH10, assume their temporary residency within a specific area of the anterior lateral plate splanchnic mesoderm, generally referred to as the primary heart field. It is a widely-held belief that early in avian cardiovascular development (HH5), both the myocardial and endocardial cells are found in this primary heart-forming region. However, recent work by Tzahor and colleagues (Milgrom-Hoffman et al., 2011) in the chick embryo indicate the endocardial-forming field is situated outside of the cardiac crescent, and is continuous with the vascular endothelial plexus. Their work suggests an endothelial origin of the endocardium. Thus, controversy still exists over when and where the two avian cardiac lineages and the endothelial lineage(s) are first specified and the exact location and extent of the respective precursor fields (Cui et al., 2009;

reviewed in Harris and Black, 2010). In contrast, in zebrafish the endocardium originates from a distinct region in the anterior cardiogenic mesoderm, located more rostral than the source of myocardial progenitors (Bussmann et al., 2007; Schoenebeck et al., 2007).

Regardless of when and where the endocardial precursors are first specified, the endocardium arises through a process of de novo vasculogenesis from a distinct population of precursors in the anterior lateral plate mesoderm. We have demonstrated that pre-endocardial cells and vascular endothelial cells are separated by a sharp horseshoe-shaped boundary within the anterior LPM (Fig. 6). We believe that cells located on the “endocardial” side of this boundary are subject to the midline-directed tissue movement. While we are not in a position to claim that position fate is the only determinant of these two cohorts of Tie1 + precursors, we do believe that position fate plays an important role in the formation of blood vessels versus the endocardium.

The endocardial tube is formed from the bilateral field of endocardial precursors by the centripetal movement of these cells along the posterior margin of the anterior intestinal portal; importantly the cells positioned at the midline and lateral margins appear to move with the same speed. After HH10, as the endocardial tube continues to elongate, we see cells contributing to the endocardium from the closely-associated vascular plexus located ventral to the foregut endoderm (Supplemental Fig. 6).

By developing a system of substages between HH8 – to 11 (Supplemental Fig. 5), which better characterize endocardial morphology, we show the reproducibility in the progression of endocardial formation from a scattered pool of precursors initially located between the anterior LPM and endoderm. The seven substages, which we refer to as ES1–ES7, are distinguishable from one another by the characteristics of the Tie+ positive cells and the morphological events that are occurring concomitant with endocardial morphogenesis. As discussed in detail in the Results section, defining characteristics included the number, location and organization of the Tie+ endocardial precursors as well as the general morphology of the cranial embryo as it relates to elongation of the foregut, regression of the anterior intestinal portal, and elongation of the endocardial tube and cardiac bending.

#### Tissue and active cell movements

The most likely interpretation for the shared large-scale movement pattern between the two ECM components and endocardial progenitors is a model whereby the whole tissue (cells and the associated ECM as a composite material) moves and deforms in response to mechanical forces, exerted by cells within the heart field or in adjacent tissue layers. The finding that microinjected inert objects also translocate to the forming heart, in an identical manner, is entirely consistent with such a view. In previous works, we have operationally defined “tissue motion” as the coordinated movements of cells and their local ECM environment (Czirók et al., 2006; Perryn et al., 2008; Sato et al., 2010; Zamir et al., 2006, 2008). Displacements associated with tissue motion are correlated over large distances, up to a several hundred microns (Szabó et al., 2011). As we have shown in this work, active motility of endocardial progenitors, defined as the difference between the local cell and ECM displacements, is much smaller and more random than the movements characterizing tissue deformation. The randomness and smaller scale of active cell movements were recently also demonstrated for cells of the pre-somitic mesoderm (Bénazéraf et al., 2010).

Although our work clearly shows that tissue motion predominates in the repositioning of pre-endocardial cells to form the midline endocardial tube, it is important to determine what role the cell autonomous motility plays in endocardial morphogenesis. The random active cell movements can play an important role in the reorganization of the local ECM. At later stages of cardiac development, the observed directional component of the autonomous motion may be critical for the

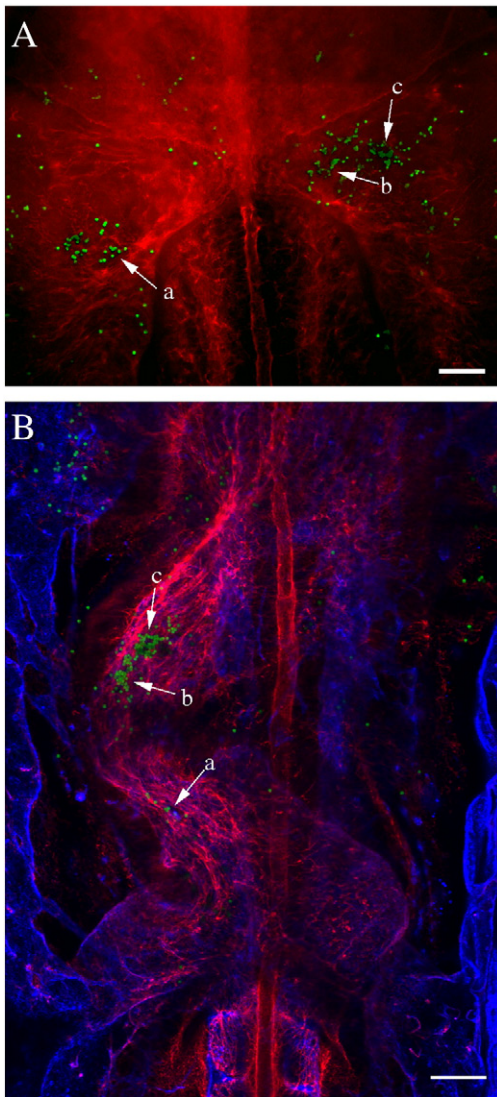


**Fig. 8.** Tissue motion transfers passive objects to the site of cardiogenesis. A: Microinjected latex beads (green) within a HH8 – embryo, also immunolabeled for fibrillin-2 (red). Arrows a–c indicate groups of beads that were incorporated in the forming heart tube at HH12 (see Movie S9). B: Confocal micrograph of the same embryo at HH12, immunostained with QH1 antibody. A 24  $\mu\text{m}$  thick confocal stack through the heart tube was obtained along the dorso-ventral axis. The image shown is a maximum intensity projection, beads are shown in green, fibrillin-2 in red and QH1 in blue. As determined by tracking the beads through the time-lapse image sequence, arrows a–c indicate identical groups of beads in both panels. In agreement to our results shown in Figs. 2 and 3, the group of beads indicated by (a) entered the heart tube from the caudal end, and those indicated by (b) and (c) were included in the forming heart from the cranial pole.

precise repositioning of the precursors. The calculated autonomous speeds of 20  $\mu\text{m}/\text{h}$  are in the same range as those reported for endothelial cells moving in culture (10  $\mu\text{m}/\text{h}$ : Szabó et al., 2010, 50  $\mu\text{m}/\text{h}$ : Kouvroutoglou et al., 2000). In comparison, the active movement of gastrulating mesoderm cells is somewhat faster, in the range of 60  $\mu\text{m}/\text{h}$  (Zamir et al., 2006).

The driving forces for endocardial progenitor motion are likely to differ between avian (and other higher vertebrate) embryos and zebrafish; the latter model system has been used for studies of endocardial morphogenesis in a number of recent studies (Bussmann et al., 2007; Fish et al., 2011; Schoenebeck et al., 2007). Even though many aspects of cardiac development are very similar in zebrafish and avians (reviewed in Alexander and Stainier, 1999), some significant differences exist and must be taken into account. For instance, Bussmann et al. (2007) described two facets of endocardial morphogenesis distinct in zebrafish and higher vertebrates. First, unlike in avian embryos, zebrafish endocardial progenitors engage in posterior movements from the discrete region they occupy in the cardiogenic mesoderm to the site of the heart tube assembly. Second, in contrast to our results in the avian embryo, in fish embryos, endocardial precursors appear to rapidly migrate to the site of heart tube formation, where they arrive and form a sheet prior to the formation of bilateral myocardial primordia and initiation of their midline-directed movements (Bussmann et al., 2007). After their arrival at the ventral midline, endocardial cells direct angular movements of myocardial progenitors in zebrafish (Holtzman et al., 2007). Bussmann et al. also pointed out the virtual absence of dynamic imaging-based studies of endocardial progenitor motion in avian or mouse embryos, a gap that the current study aims to help fill.

In contrast to zebrafish endocardial morphogenesis, assembly of the avian endocardium occurs simultaneously with that of the myocardium, and both cell types simultaneously engage in antero-medial motion. This points to myocardial movements as the potential driving force for tissue motion, a force in turn that leads to endocardial cell displacements. The coordinated movements of myocardial cell populations were indeed suggested to “drive” the formation of the heart tube in chick (DeHaan, 1963) and in rat (Suzuki et al., 1995). However, since the endocardial cells are clearly moving with the associated ECM, such a mechanism would require another adhesion substrate, i.e., a layer of ECM distinct from the one associated with the endocardial precursors. Our monoclonal antibody labeling of endogenous fibrillin-2 and fibronectin do not show such distinct ECM layers in optical or physical sections. Potentially myocardial progenitors could move relative to ECM components not fluorescently labeled in this study. However, given the importance of fibronectin for myocardial movements (Linask and Lash, 1986; Trinh and Stainier, 2004) one would expect myocardial progenitors to rely on it as the adhesion substrate, at least in part. Surprisingly though, our recent preliminary data suggest that myocardial cell movements relative to fibronectin ECM are relatively small, and are very similar in speed and magnitude to endocardial precursor active movements.

Another tissue candidate potentially responsible for driving tissue movement in the anterior embryo is the endoderm. This function would complement an important signaling role of the endoderm in cardiac development, reported for zebrafish, *Xenopus*, chick and mouse (Lough and Sugi, 2000). In avian embryos (as well as mouse and human), the endoderm undergoes a series of morphogenetic movements, involving dramatic tissue folding events, to form the gut tube. Elongation of the formed gut involves rapid posterior movement of the anterior intestinal portal (AIP), concomitant with narrowing of the endodermal tube. The foregut and the heart tube are physically associated via a mesentery (dorsal mesocardium) throughout the initial cardiac assembly stages, making the movements of the endoderm and cardiogenic mesoderm tightly coupled.

The mechanisms that drive foregut assembly and elongation remain poorly understood in avian and mammalian systems. Stalsberg and DeHaan (1968) suggested that in avians, the foregut elongates as a

result of tension applied at the anterior intestinal portal, and the tension arises from the regression of the primitive streak and elongation of the notochord. The same force may be transmitted to the subjacent splanchnic mesoderm (including cardiogenic mesoderm), acting to drag that layer medially and caudally (Stalsberg and DeHaan, 1968). In the mouse, foregut and heart tube formation were suggested to depend upon visceral extraembryonic endoderm movements (Narita et al., 1997). Further, in studies in which the transcription factor GATA4 (expressed in precardiac splanchnic mesoderm and foregut endoderm) has been knocked out, visceral endoderm defects, gut malformations, and abnormal heart morphogenesis result (Kuo et al., 1997; Molkentin et al., 1997; discussed in Rojas et al., 2010). The authors demonstrate that GATA4 has a role in the formation of the anterior intestinal portal, and subsequent foregut and heart tube morphogenesis via a role in lateral to ventral folding. The mechanism of gut formation is different in zebrafish and *Xenopus*, where the endoderm forms from a “rod” of cells, which develops a lumen and gives rise to the gut tube (reviewed in Spence et al., 2011).

Recently the local residual stresses were mapped in the early epiblast and a tissue mechanical model was proposed for headfold formation (Varner et al., 2010). We expect an approach similar to Varner and colleagues would aid in our understanding of the underlying mechanisms of foregut formation and its possible role in driving cardiac progenitor displacements to the ventral midline.

The work presented here lays the basis for our ongoing and future studies aimed at the characterization of the relative movements of endocardial and myocardial progenitor cells, their ECM environment and surrounding non-cardiac cell populations in live developing avian embryos. In addition to experimental embryology and imaging approaches, it is clear that mathematical modeling will prove useful in determining what biophysical mechanism(s), such as force generation, are necessary to form the cardiac tube at the midline.

Supplementary materials related to this article can be found online at doi:10.1016/j.ydbio.2011.12.036.

## Acknowledgments

The authors would like to thank Dr. Charles Little for his insightful comments and for his assistance preparing the schematics. We also wish to thank Ms. Pat St John for her expert technical assistance in optimizing the conditions for cryosectioning avian embryonic hearts.

This work was supported by NIH grants HL085694 (BJR); HL087136 (AC); the Hungarian Research Fund OTKA K72664 (AC); the G. Harold & Leila Y. Mathers Charitable Foundation (BJR, AC), a Faculty Scholar Award supported by P20 RR016475 from the NCR (BJR) and a Biomedical Research Training Program award (AA).

## References

- Abu-Issa, R., Kirby, M.L., 2008. Patterning of the heart field in the chick. *Dev. Biol.* 319, 223–233.
- Alexander, J., Stainier, D.Y.R., 1999. Mutations affecting cardiac development in zebrafish. In: Harvey, R.P., Rosenthal, N. (Eds.), *Heart Development*. Academic Press, San Diego, London, Boston, New York, Sydney, Tokyo, Toronto, pp. 91–110.
- Bellairs, R., Osmond, M., 2005. *Atlas of Chick Development*, 2nd ed. Academic Press.
- Bénazéraf, B., Francois, P., Baker, R.E., Denans, N., Little, C.D., Pourquié, O., 2010. A random cell motility gradient downstream of FGF controls elongation of an amniote embryo. *Nature* 466 (7303), 248–252.
- Bowers, S.L., Baudino, T.A., 2010. Laying the groundwork for growth: cell–cell and cell–ECM interactions in cardiovascular development. *Birth Defects Res. C Embryo Today* 90 (1), 1–7.
- Bussmann, J., Bakkers, J., Schulte-Merker, S., 2007. Early endocardial morphogenesis requires *Scf/Tal1*. *PLoS Genet.* 3, e140.
- Chapman, S.C., Collignon, J., Schoenwolf, G.C., Lumsden, A., 2001. Improved method for chick whole-embryo culture using a filter paper carrier. *Dev. Dyn.* 220, 284–289.
- Cui, C., Chevrouret, T.J., Lansford, R.D., Moreno-Rodriguez, R.A., Shultheiss, T.M., Rongish, B.J., 2009. Dynamic positional fate map of the primary heart-forming region. *Dev. Biol.* 332, 212–222.
- Czirók, A., Zamir, E.A., Filla, M.B., Little, C.D., Rongish, B.J., 2006. Extracellular matrix macro-assembly dynamics in early vertebrate embryos. *Curr. Top. Dev. Biol.* 73, 237–258.

- Czirók, A., Rupp, P.A., Rongish, B.J., Little, C.D., 2002. Multi-field 3D scanning light microscopy of early embryogenesis. *J. Microsc.* 206, 209–217.
- Czirók, A., Rongish, B.J., Little, C.D., 2004. Extracellular matrix dynamics during vertebrate axis formation. *Dev. Biol.* 268, 111–122.
- DeHaan, R.L., 1963. Migration patterns of the precardiac mesoderm in the early chick embryo. *Exp. Cell Res.* 29, 544–560.
- DeRuiter, M.C., Poelmann, R.E., Mentink, M.M., Vaniperen, L., Gittenberger-De Groot, A.C., 1993. Early formation of the vascular system in quail embryos. *Anat. Rec.* 235 (2), 261–274.
- Drake, C.J., Davis, L.A., Walters, L., Little, C.D., 1990. Avian vasculogenesis and the distribution of collagens I, IV, laminin, and fibronectin in the heart primordia. *J. Exp. Zool.* 255 (3), 309–322.
- Drake, C.J., Wessels, A., Trusk, T., Little, C.D., 2006. Elevated vascular endothelial cell growth factor affects mesocardial morphogenesis and inhibits normal heart bending. *Dev. Dyn.* 235 (1), 10–18.
- Drocco, J.A., Grimm, O., Tank, D.W., Wieschaus, E., 2011. Measurement and perturbation of morphogen lifetime: effects on gradient shape. *Biophys. J.* 101 (8), 1807–1815.
- Fish, J.E., Wythe, J.D., Xiao, T., Bruneau, B.G., Stainier, D.Y., Srivastava, D., Woo, S., 2011. A Slit/miR-218/Robo regulatory loop is required during heart tube formation in zebrafish. *Development* 138 (7), 1409–1419.
- Fontana, L., Chen, Y., Prijatelj, P., Sakai, T., Fassler, R., Sakai, L.Y., Rifkin, D.B., 2005. Fibronectin is required for integrin alphavbeta6-mediated activation of latent TGF-beta complexes containing LTBP-1. *FASEB J.* 19, 1798–1808.
- Hamburger, V., Hamilton, H.L., 1951. A series of normal stages in the development of the chick embryo. *J. Morphol.* 88, 49–92.
- Harris, I.S., Black, B.L., 2010. Development of the endocardium. *Pediatr. Cardiol.* 31 (3), 391–399.
- Holtzman, N.G., Schoenebeck, J.J., Tsai, H.J., Yelon, D., 2007. Endocardium is necessary for cardiomyocyte movement during heart tube assembly. *Development* 134, 2379–2386.
- Hossain, M.J., Whelan, P.F., Czirók, A., Ghita, O., 2011. An active particle-based tracking framework for 2D and 3D time-lapse microscopy images. *Conf. Proc. IEEE Eng. Med. Biol. Soc.* 6613–6618.
- Ishii, Y., Langberg, J., Rosborough, K., Mikawa, T., 2009. Endothelial cell lineages of the heart. *Cell Tissue Res.* 335, 67–73.
- Kitten, G.T., Markwald, R.R., Bolender, D.L., 1987. Distribution of basement membrane antigens in cryopreserved early embryonic hearts. *Anat. Rec.* 217 (4), 379–390.
- Kouvroukoglou, S., Dee, K.C., Bizios, R., McIntire, L.V., Zygorakis, K., 2000. Endothelial cell migration on surfaces modified with immobilized adhesive peptides. *Biomaterials* 21 (17), 1725–1733.
- Krug, E.L., Runyan, R.B., Markwald, R.R., 1985. Protein extracts from early embryonic hearts initiate cardiac endothelial cytodifferentiation. *Dev. Biol.* 112 (2), 414–426.
- Kuo, C.T., Morrisey, E.E., Anandappa, R., Sigrist, K., Lu, M.M., Parmacek, M.S., Soudais, C., Leiden, J.M., 1997. GATA4 transcription factor is required for ventral morphogenesis and heart tube formation. *Genes Dev.* 11, 1048–1060.
- Leiss, M., Beckmann, K., Giros, A., Costell, M., Fassler, R., 2008. The role of integrin binding sites in fibronectin matrix assembly in vivo. *Curr. Opin. Cell Biol.* 20, 502–507.
- Lillie, Frank R., 1930. *The Development of the Chick*, 2nd ed. Henry Holt and Co., New York.
- Linask, K.K., 2003. Regulation of heart morphology: current molecular and cellular perspectives on the coordinated emergence of cardiac form and function. *Birth Defects Res. C Embryo Today* 69 (1), 14–24.
- Linask, K.K., Lash, J.W., 1986. Precardiac cell migration: fibronectin localization at mesoderm–endoderm interface during directional movement. *Dev. Biol.* 114 (1), 87–101.
- Little, C.D., Drake, C.J., 2000. Whole-mount immunolabeling of embryos by microinjection. Increased detection levels of extracellular and cell surface epitopes. *Methods Mol. Biol.* 135, 183–189.
- Little, C.D., Rongish, B.J., 1995. The extracellular matrix during heart development. *Experientia* 51, 873–882.
- Lough, J., Sugi, Y., 2000. Endoderm and heart development. *Dev. Dyn.* 217 (4), 327–342.
- Milgrom-Hoffman, M., Harrelson, Z., Ferrara, N., Zelzer, E., Evans, S.M., Tzahor, E., 2011. The heart endocardium is derived from vascular endothelial progenitors. *Development* 138 (21), 4777–4787.
- Molkentin, J.D., Lin, Q., Duncan, S.A., Olson, E.N., 1997. Requirement of the transcription factor GATA4 for heart tube formation and ventral morphogenesis. *Genes Dev.* 11, 1061–1072.
- Narita, N., Bielinska, M., Wilson, D.B., 1997. Wild-type endoderm abrogates the ventral developmental defects associated with GATA-4 deficiency in the mouse. *Dev. Biol.* 189 (2), 270–274.
- Pardanaud, L., Altmann, C., Kitos, P., Dieterlen-Lievre, F., Buck, C.A., 1987. Vasculogenesis in the early quail blastodisc as studied with a monoclonal antibody recognizing endothelial cells. *Development* 100, 339–349.
- Perryn, E.D., Czirók, A., Little, C.D., 2008. Vascular sprout formation entails tissue deformations and VE-cadherin-dependent cell-autonomous motility. *Dev. Biol.* 313, 545–555.
- Rojas, A., Schachterle, W., Xu, S.-M., Martin, F., Black, B.L., 2010. Direct transcriptional regulation of Gata4 during early endoderm specification is controlled by FoxA2 binding to an intronic enhancer. *Dev. Biol.* 346, 346–355.
- Sato, Y., Poynter, G., Huss, D., Filla, M.B., Czirók, A., Rongish, B.J., Little, C.D., Fraser, S.E., Lansford, R., 2010. Dynamic analysis of vascular morphogenesis using transgenic quail embryos. *PLoS One* 5, e12674.
- Schoenebeck, J.J., Keegan, B.R., Yelon, D., 2007. Vessel and blood specification override cardiac potential in anterior mesoderm. *Dev. Cell* 13 (2), 254–267.
- Spence, J.R., Lauf, R., Shroyer, N.F., 2011. Vertebrate intestinal endoderm development. *Dev. Dyn.* 240, 501–520.
- Stalsberg, H., DeHaan, R.L., 1968. Endodermal movements during foregut formation in the chick embryo. *Dev. Biol.* 18 (2), 198–215.
- Stenzel, D., Lundkvist, A., Sauvaget, D., Busse, M., Graupera, M., van der Flier, A., Wijelath, E.S., Murray, J., Sobel, M., Costell, M., Takahashi, S., Fassler, R., Yamaguchi, Y., Gutmann, D.H., Hynes, R.O., Gerhardt, H., 2011. Integrin-dependent and -independent functions of astrocytic fibronectin in retinal angiogenesis. *Development* 138, 4451–4463.
- Suzuki, H.R., Solorsh, M., Baldwin, H.S., 1995. Relationship between fibronectin expression during gastrulation and heart formation in the rat embryo. *Dev. Dyn.* 204 (3), 259–277.
- Szabó, A., Rupp, P.A., Rongish, B.J., Little, C.D., Czirók, A., 2011. Extracellular matrix fluctuations during early embryogenesis. *Phys. Biol.* 8, 045006.
- Szabó, A., Unnep, R., Méhes, E., Twal, W.O., Argraves, W.S., Cao, Y., Czirók, A., 2010. Collective cell motion in endothelial monolayers. *Phys. Biol.* 7 (4), 046007 (PMID: 21076204).
- Trinh, L.A., Stainier, D.Y., 2004. Fibronectin regulates epithelial organization during myocardial migration in zebrafish. *Dev. Cell* 6, 371–382.
- Varner, V.D., Voronov, D.A., Taber, L.A., 2010. Mechanics of head fold formation: investigating tissue-level forces during early development. *Development* 137 (22), 3801–3811 (Epub 2010 Oct 7).
- Wijelath, E.S., Murray, J., Rahman, S., Patel, Y., Ishida, A., Strand, K., Aziz, S., Cardona, C., Hammond, W.P., Savidge, G.F., Rafii, S., Sobel, M., 2002. Novel vascular endothelial growth factor binding domains of fibronectin enhance vascular endothelial growth factor biological activity. *Circ. Res.* 91, 25–31.
- Yu, S.R., Burkhardt, M., Nowak, M., Ries, J., Petrasek, Z., Scholpp, S., Schwill, P., Brand, M., 2009. Fgf8 morphogen gradient forms by a source-sink mechanism with freely diffusing molecules. *Nature* 461, 533–536.
- Zamir, E.A., Czirók, A., Rongish, B.J., Little, C.D., 2005. A digital image-based method for computational tissue fate mapping during early avian morphogenesis. *Ann. Biomed. Eng.* 33, 854–865.
- Zamir, E.A., Czirók, A., Cui, C., Little, C.D., Rongish, B.J., 2006. Mesodermal cell displacements during avian gastrulation are due to both individual cell-autonomous and convective tissue movements. *Proc. Natl. Acad. Sci. U. S. A.* 103, 19806–19811.
- Zamir, E.A., Rongish, B.J., Little, C.D., 2008. The ECM moves during primitive streak formation—computation of ECM versus cellular motion. *PLoS Biol.* 6, e247.